



HAL
open science

Universal switched state-space representation for model predictive control of power converters

Samuel Jupin, Ionel Vechiu, Gerardo Tapia-Otaegui

► To cite this version:

Samuel Jupin, Ionel Vechiu, Gerardo Tapia-Otaegui. Universal switched state-space representation for model predictive control of power converters. Electric Power Systems Research, 2020, 180, pp.106120. 10.1016/j.epsr.2019.106120 . hal-02390618

HAL Id: hal-02390618

<https://hal.science/hal-02390618>

Submitted on 21 Jul 2022

HAL is a multi-disciplinary open access archive for the deposit and dissemination of scientific research documents, whether they are published or not. The documents may come from teaching and research institutions in France or abroad, or from public or private research centers.

L'archive ouverte pluridisciplinaire **HAL**, est destinée au dépôt et à la diffusion de documents scientifiques de niveau recherche, publiés ou non, émanant des établissements d'enseignement et de recherche français ou étrangers, des laboratoires publics ou privés.



Distributed under a Creative Commons Attribution - NonCommercial 4.0 International License

Universal Switched State-Space Representation for Model Predictive Control of Power Converters

Samuel Jupin^{a, b, *}, Ionel Vechiu^a, Gerardo Tapia-Otaegui^b

a: Univ. Bordeaux, ESTIA INSTITUTE OF TECHNOLOGY, 97 allée Théodore Monod 64210 Bidart France

b: University of the Basque Country UPV/EHU, Department of Automatic Control and Systems Engineering, Faculty of Engineering, Gipuzkoa, Plaza de Europa 1, 20018 San Sebastián, Spain

Abstract— In order to enable interoperability of Renewable Energy Sources (RES) with smart grids, power converters together with high speed and high accuracy controllers are needed. The use of power converters and of their associated enhanced control techniques both ensures the interface of intermittent energy sources with the grid and supports the grid with ancillary services, while also improving the power quality and stability during different grid disturbances. Therefore, to address all these important issues, the controllers applied to power converters are more and more complex, and rely on precise models. This paper focuses on formalizing a universal method to generate accurate state-space models for any controlled power converter, down to the level of its power switches. This model representation is particularly useful for direct power controllers, as they bypass the conventional modulation techniques to increase reliability and efficiency of power converters. The accuracy of the proposed method is demonstrated on a 4 Leg 3 Level Flying Capacitor (4L-3L FC) topology associated with a LCL filter through several simulation results.

Index Terms—Switched state-space model, power converters, multi-level power converters, model predictive control, stability.

List of Abbreviations

4-Leg 3-Level Flying Capacitor (4L-3L FC)

Continuous SSSR (CSSSR)

Discrete SSSR (DSSSR)

Flying Capacitor (FC)

Model Predictive Control (MPC)

Renewable Energy Sources (RES)

Simscape Power Systems™ model (SPSM)

Switched State-Space Representation (SSSR)

Zero-Order Hold (ZOH)

Corresponding author: Samuel Jupin, Univ. Bordeaux, ESTIA Institute of technology, University of the Basque Country UPV/EHU, s.jupin@estia.fr

© 2019 published by Elsevier. This manuscript is made available under the CC BY NC user license

<https://creativecommons.org/licenses/by-nc/4.0/>

1. Introduction

The evolution of the electrical grid relies heavily on power conversion to maintain power quality, stability, and to provide various ancillary services, for an overall reliability. Upon the last decade, RES have been massively integrated into the electrical grid, using power converters [1], [2].

The maturation of the distribution and conversion technologies brings new more rigorous operational criteria to the table. These requirements include efficiency and reliability of the power converters, which are used not only to interface several RES and storage systems with the grid to make them interoperable, but also to realize precise functionalities and to optimize global operation [3], [4]. Despite the advantages offered by the RES, considered efficient power sources providing sustainable and clean energy, the connection of large RES power plants to the grid with high penetration could be subject to several operational problems [5]. In this context, power converters —through advanced control strategies— could play an important role in order to improve power quality and grid stability [6], [7].

Power converters are hybrid systems: they act discreetly on continuous values through their power semiconductor switching devices. This hybrid nature leads to control difficulties, usually bypassed thanks to the modulation strategies [8], [9]. In fact, an important number of the previously evoked control objectives is related to the exact command of the switching devices [3]. However, relying on modulation on these circumstances can lead to major modifications of the control structure.

In order to further improve efficiency and reliability of power converters without recurring deep modifications of the control architectures, it is important to provide additional intelligence to their control, down to the level of power switches. Recently, a variety of advanced controls has been developed to improve the operation of power converters, such as sliding-mode control [10]–[13] or MPC [14]–[17]. Both methods offer the capacity to

overcome the hybrid nature obstacle directly with the controller, therefore enabling a deeper control of the system. Nevertheless, they strongly depend on the definition of models and equations of the systems to perform optimally.

As previously suggested, power converters cannot be modeled via conventional linear methods. A common approach relies on defining models for a very specific application or topology, be it flying capacitor [18], neutral-point clamped [19], [20] or any other, without considering the various particularities that come with these unordinary models.

This paper formalizes a modeling method, occasionally applied to power converters, that bears great potential for control design. This method relies on SSSR, a non-linear modeling strategy commonly applied to other hybrid systems, mechanical or chemical for example, and can intuitively be associated with operational research algorithms to perform optimization, henceforth MPC.

A canonical definition is proposed for any controlled power converter, and the stability is investigated for this particular description. A simple and effective method to determine the stability of such systems is presented. The model developed is adapted to all power converters and designed to be coupled with an optimization algorithm to form an MPC control scheme. This combination leads to a controller able to bypass the conventional modulation strategies, therefore increasing reliability and efficiency, for any power converter. To demonstrate the validity of the method, the SSSR of a 4L-3L FC associated with a LCL grid filter is determined and compared to a more precise simulation tool.

The paper is organized as follows: Section 2 presents the formalism and defines the modeling method, with results on stability and a discussion on limitations and advantages. Section 3 focuses on the consequences of the adaptation of this method to power converters, while Section 4 illustrates the method and its properties on the specific case of 4L-3L FC. Finally, Section 5 summarizes the main points of this paper.

2. Switched State-Space Representation

2.1. General presentation

SSSR is a modeling method used when considering hybrid systems combining a discrete definition with continuous quantities. Typical examples include chemical processes, vehicles, parameter-varying systems, etc. The overall system is described by a set of continuous subsystems, associated to the various events, σ , affecting the system. This means that instead of the ordinary dynamics, as presented in (1), the SSSR model is portrayed by (2).

$$\dot{\mathbf{x}}(t) = \mathbf{A}\mathbf{x}(t) + \mathbf{B}\mathbf{u}(t) + \mathbf{E}\mathbf{d}(t) \quad (1)$$

$$\dot{\mathbf{x}}(t) = \mathbf{A}_{\sigma(t)}\mathbf{x}(t) + \mathbf{E}_{\sigma(t)}\mathbf{d}(t) \quad (2)$$

Therefore, the global “power converter” system can be described as a combination of the “power converter in position σ ” subsystems. In the case of power converters, the position is dictated by control \mathbf{u} , which leads to

$$\dot{\mathbf{x}}(t) = \mathbf{A}(\mathbf{u}(t))\mathbf{x}(t) + \mathbf{E}(\mathbf{u}(t))\mathbf{d}(t). \quad (3)$$

This equation highlights the subsystem definition: for each possible control \mathbf{u} , the $\mathbf{A}(\mathbf{u})$ and $\mathbf{E}(\mathbf{u})$ matrices are constant and lead to a usual linear state-space representation as in (1). This allows prediction and modeling as usual, and can be associated to an optimal graph navigation algorithm with the aim of developing a general MPC scheme adapted to any power converter topology.

The same reasoning can be applied to other formalisms such as port-controlled Hamiltonian, as in [21].

2.2. Stability

The stability of each subsystem can be determined by studying the eigenvalues of its

corresponding submatrix: if and only if all the eigenvalues of the \mathbf{A} matrix own strictly negative real parts, then the system described by said matrix is asymptotically stable. In contrast, if one or more eigenvalues exhibit strictly positive real parts, the system turns out to be unstable. Finally, if one or more eigenvalues are placed on the imaginary axis and the rest show strictly negative real parts, stability cannot be determined.

However, establishing the stability of each subsystem is not sufficient to demonstrate the stability of the overall system [22]. In fact, even if all submatrices correspond to asymptotically stable subsystems, it may exist a sequence that renders the global system unstable. Similarly, even if a system is comprised only of unstable submatrices, there might be a series of commutation stabilizing it [23], [24].

Therefore, two definitions of stability for SSSRs are found. The first one deals with the existence of a stabilizing sequence, whereas the second focuses on stability for any commutation sequence. The latter definition requires all subsystems to be asymptotically stable, but this condition alone is not sufficient. Moreover, given that the case of filter-connected power converters leads to just a few stable subsystems, this aspect is not to be covered here. However, it is interesting to demonstrate the existence of a sequence stabilizing the system, as if such a sequence does not exist, it is useless to consider applying control.

According to Lyapunov's theorem, finding a convex linear combination of the subsystems is sufficient to prove the existence of a commutation sequence that stabilizes the overall system [25], [26]. This amounts to finding

$$\alpha_i > 0; \sum_{i=1}^N \alpha_i = 1, \quad (4)$$

with N being the total number of subsystems, such that the equivalent system represented by matrix

$$\mathbf{A}_{eq} = \sum_{i=1}^N \alpha_i \mathbf{A}_i \quad (5)$$

is stable. Accordingly, proving that such an equivalent system is stable is sufficient to demonstrate the existence of a switching sequence stabilizing the system. However, this method does not provide the said commutation sequence.

2.3. Control-oriented model

The model proposed in (3) is designed to be coupled with advanced MPC algorithms to directly control the switches of power converters. Consequently, it focuses on the effects of these switches in the model. A few simplifications are performed to reduce the complexity of the prediction. The most significant one is the way the power switches are considered ideal. Judging from the time period considered and the significant computation savings, the differences caused by this hypothesis are negligible.

Additionally, the model proposed is the transition of submodels from one to another. Each transition presents a risk. If, for any reason, the state given by a submodel right before a transition is not identical to the one of the real system, the resulting bias becomes an initialization error for the following submodel. This error can come from wrong parameters, discretization, inadequate modeling... and will end up propagating randomly with time and transitions, unpredictably accumulating or vanishing. For this reason, it is not recommended to use this modeling method in open loop for long periods of time, as bias may be introduced and propagated. Even absolutely perfect submodels become heavily biased after a few thousand transitions. For longer times, an averaged model may be preferred.

Nevertheless, when considering direct control of the switches of power converters, thousands of transitions in open loop is a mirage and closed-loop is favored, then the proposed model is adequate. Indeed, this model is used for all the predictive aspects of the MPC algorithm, whose prediction horizon is limited to less than ten sample times. For such a

period of time, the limitations of the proposed model are not perceived. Furthermore, MPC is recognized for being particularly robust [27], which emphasizes the purpose of this model to be associated with MPC for closed-loop direct control of the switches of power converters.

3. Modeling methodology for power converters

3.1. Form of the SSSR

From Fig. 1, it can be concluded that the most general presentation of power converters shows five aspects. First, the two outer buses, whose behavior is considered external to the converter itself: their dynamics are not studied and their respective actions on the converter are regarded as uncontrolled inputs. Then, the corresponding filters or links, containing a number of capacitors and inductors, to which state variables are associated. The bridge between the two groups of state variables is made through the commutation cells, which may add state variables for some topologies. The control is performed by the open/close orders transmitted to each IGBT of the commutation cells.

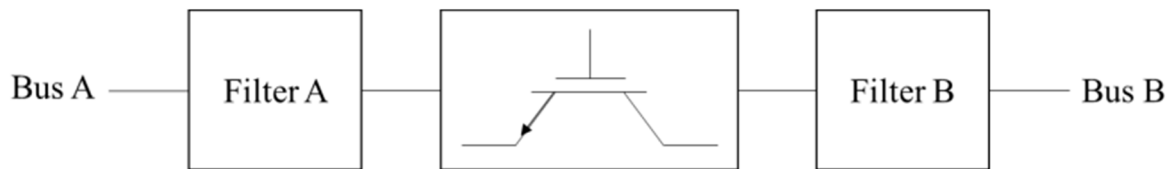


Fig. 1. General context of power conversion. Two buses, A and B, are connected through a filter + commutation cell system.

Therefore, the state vector is divided in three parts: the \mathbf{x}_A states corresponding to the A side filter, the \mathbf{x}_{con} ones related to the internal components of the converter, and the \mathbf{x}_B states coming from the other side's filter. Similarly, the uncontrolled input vector is formed by the \mathbf{d}_A inputs generated by the A side and the \mathbf{d}_B ones spawned by the B side. The control vector \mathbf{u} is an image of the switches' positions. The input, control and state vectors are presented in (6).

$$\mathbf{d} = \begin{bmatrix} \mathbf{d}_A \\ \mathbf{d}_B \end{bmatrix}; \quad \mathbf{u} = \mathbf{f}(\mathbf{switch}); \quad \mathbf{x} = \begin{bmatrix} \mathbf{x}_A \\ \mathbf{x}_{con} \\ \mathbf{x}_B \end{bmatrix} \quad (6)$$

By design, it is possible for some of these sub-vectors to be empty, depending on both the topology and the context.

The \mathbf{f} function is chosen to accurately depict the impact of the switching states on the connection between the A and B hands. For energy management applications, which need to precisely perceive the quantity of energy passing through every gate, \mathbf{f} can be specified as bijective. Nevertheless, though surjective, this function is not necessarily injective, as distinct switching positions can lead to the same link.

With this definition of the state variables, the \mathbf{A} matrix can be divided in blocks as shown in (7).

$$\mathbf{A}(\mathbf{u}) = \begin{bmatrix} \mathbf{A}_{AA} & \mathbf{A}_{Acon}(\mathbf{u}) & \mathbf{A}_{AB}(\mathbf{u}) \\ \mathbf{A}_{conA}(\mathbf{u}) & \mathbf{A}_{concon} & \mathbf{A}_{conB}(\mathbf{u}) \\ \mathbf{A}_{BA}(\mathbf{u}) & \mathbf{A}_{Bcon}(\mathbf{u}) & \mathbf{A}_{BB} \end{bmatrix} \quad (7)$$

Notably, the diagonal blocks do not depend on the commutation orders, while all the remaining submatrices are defined as functions of the switching control. The \mathbf{A}_{AA} and \mathbf{A}_{BB} blocks represent the dynamics of the filters, while all the other blocks contain the converter's proper behavior. It is interesting to note that, by approaching the problem this way, the \mathbf{E} input matrix in (8) does not depend on the commutation.

$$\dot{\mathbf{x}} = \mathbf{A}(\mathbf{u})\mathbf{x} + \mathbf{E}\mathbf{d} \quad (8)$$

3.2. Modeling

Fixing the position of the switches contained within a power converter commutation cell leads to an electrical circuit that can be linearly modeled by making use of both the elementary equations of its components and Kirchhoff's laws. Therefore, given a position k , a

specific \mathbf{A}_k matrix is defined, hence leading to subsystem

$$\dot{\mathbf{x}} = \mathbf{A}_k \mathbf{x} + \mathbf{E} \mathbf{d} \quad (9)$$

Then, all sets are assembled according to the theorem of superposition. This method calls for combinatory logic. Indeed, considering that all possible controls for each commutation cell are mutually exclusive, the command can be expressed through logic binary variables obeying elementary laws of logic. In particular, assuming that U_{cell} is the set of the N_{poss} possible switching states for a commutation cell, it turns out that

$$\mathbf{u}_k \in U_{cell}; \quad \sum_{k=1}^{N_{poss}} \mathbf{u}_k = 1. \quad (10)$$

From there on, all the subsystems represented by (9) can be added up as follows:

$$\sum_{k=1}^{N_{poss}} \mathbf{u}_k \dot{\mathbf{x}} = \sum_{k=1}^{N_{poss}} \mathbf{u}_k (\mathbf{A}_k \mathbf{x} + \mathbf{E} \mathbf{d}), \quad (11)$$

which, by virtue of (10), turns into

$$\dot{\mathbf{x}} = \left(\sum_{k=1}^{N_{poss}} \mathbf{u}_k \mathbf{A}_k \right) \mathbf{x} + \mathbf{E} \mathbf{d}. \quad (12)$$

Given that equations (10)–(12) are representative of a single cell, Kirchhoff's current law is thus applied so as to link all the converter commutation cells to one another. Indeed, once equations are established for one cell, bounding them together is trivial. The resulting system is of the form

$$\dot{\mathbf{x}}(t) = \mathbf{A}(\mathbf{u}(t)) \mathbf{x}(t) + \mathbf{E} \mathbf{d}(t). \quad (13)$$

Consequently, the $\mathbf{A}(\mathbf{u})$ matrix, formed from the different \mathbf{A}_k , depicts the dynamics of power converters using a SSSR. This method relies only on the laws of electricity and is suitable for any power converter application. It is interesting to note that two-level power

converters can be expressed as in (1), but that it is impossible to do so for multi-level power converters, therefore rendering the discussed method imperative for them.

3.3. Equivalent discrete-time model definition

All the previous definitions are expressed in continuous time. However, since the control is exerted discretely, a controller designed to deal with power converters without modulation has to be discrete itself. Therefore, such a controller requires a discrete model to operate. Application of the ZOH discretization method results in an equivalent discrete-time model of the form

$$\mathbf{x}(n+1) = \mathbf{A}_d(\mathbf{u}(n))\mathbf{x}(n) + \mathbf{E}_d(\mathbf{u}(n))\mathbf{d}(n), \quad (14)$$

where n refers to the n^{th} sampling instant and

$$\mathbf{A}_d(\mathbf{u}(n)) = e^{\mathbf{A}(\mathbf{u}(n))T}; \quad \mathbf{E}_d(\mathbf{u}(n)) = \int_0^T e^{\mathbf{A}(\mathbf{u}(n))t} \mathbf{E} dt, \quad (15)$$

with T being the sample time.

The ZOH discretization method is preferred, as it leads to an equivalent discrete-time model representing the original continuous-time system exactly as perceived by a discrete controller. Yet, (15) reveals that matrix \mathbf{E}_d can no longer be considered control independent. As a matter of fact, both \mathbf{A}_d and \mathbf{E}_d are functions of control \mathbf{u} , thus implying that the number of matrices to be computed in the discrete case is roughly twice that of the continuous one. However, this additional computational burden is necessary when discrete-time control is to be implemented.

It should also be noted that stability conditions must be adapted to the discrete case. In particular, if stability is to be guaranteed, all the eigenvalues of matrix \mathbf{A}_d should lie strictly inside the unit circle of the z complex plane.

4. Case study: Flying Capacitor

4.1. Presentation of the topology and context

Together with neutral-point clamped and cascaded H-bridge, flying capacitor is one of the three main multi-level power converter topologies. Its commutation cell is characterized by the presence of internal capacitors. This component provides an additional virtual inertia to the power converter, much appreciated in case of source disturbances and of discontinuities. This welcomed feature is promising for weak grid applications but is counterbalanced by the additional price and control complexity it implies. In fact, the capacitors offer further flexibility to the power converter, as their voltage levels strongly impact both power management and smoothing issues. This is particularly esteemed for grid applications: the capacitors may absorb extra energy in case of a surplus of production and redistribute it in the opposite case.

Figure 2 sketches the system on which the case study is focused. It consists in a 4L-3L FC converter connected to the grid through a LCL filter and to the DC bus through a double capacitor DC-link. Moreover, the following method can be applied to any power conversion

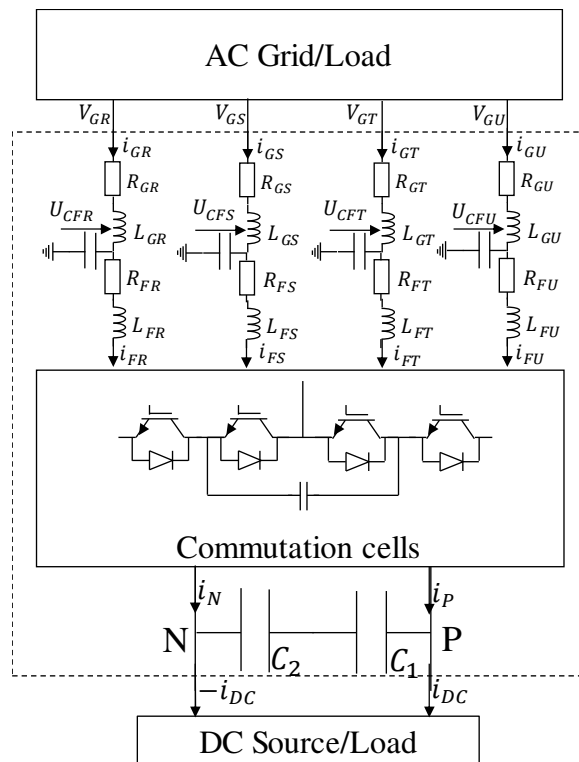


Fig. 2. Overview of the context of the study in which the modeled system is framed.

system, with no restriction, being all modeled with this method in the same way.

The four distinct ways in which the FC topology allows connecting each AC phase to the DC side can be identified from Fig. 3. For that purpose, discrete variable S_j is defined for phase j , such that it describes how connection between the said phase and the DC side is

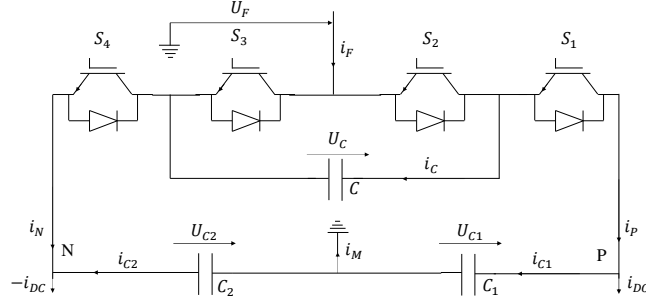


Fig. 3. Commutation cell and DC-link of the Flying Capacitor with i_F and U_F , respectively, the output current and voltage of the AC filter.

carried out. Specifically, S_j takes the $N_{poss} = 4$ possible values given next:

- S_P : the phase is bound to the P node of the DC-link
- S_N : the phase is bound to the N node of the DC-link
- S_{CP} : the phase is bound to P through the capacitor
- S_{CN} : the phase is bound to N through the capacitor

Accordingly, in this specific case, the set of possible switching states for any commutation cell U_{cell} , is given by

$$U_{cell} = \{S_P, S_N, S_{CP}, S_{CN}\}. \quad (16)$$

The correspondence between the open/closed state of the IGBTs constituting the commutation cell and the previous values is summed up in Table I, where 1 represents the closed state and 0 the open state.

TABLE I

RELATION BETWEEN THE IGBTs' STATE AND THE CONNECTION VARIABLE

S_j	S_1	S_2	S_3	S_4	Connection
S_P	1	1	0	0	P
S_N	0	0	1	1	N
S_{CP}	1	0	1	0	P, via C
S_{CN}	0	1	0	1	N, via C

In the equations provided hereafter, the first switching state of the IGBTs displayed in Table I will be represented by considering that $S_P = 1$ and $S_N = S_{CP} = S_{CN} = 0$, while the second one will be denoted by $S_N = 1$ and $S_P = S_{CP} = S_{CN} = 0$, and so on. As noticed for the generic case in (10), this implies that (17) is valid at any time, hence explicitly stating that the $N_{poss} = 4$ possible controls for the commutation cell are mutually exclusive.

$$S_P + S_N + S_{CP} + S_{CN} = 1 \quad (17)$$

4.2. SSSR of the 4L-3L FC

Considering the case of a single leg, the following equations are derived by applying Kirchhoff's laws on the adequate meshes and nodes of the circuit in Fig. 3:

$$U_F = (S_{CN} - S_{CP})U_C + (S_P + S_{CP})U_{C1} - (S_N + S_{CN})U_{C2} \quad (18)$$

$$i_C = (S_{CN} - S_{CP})i_F \quad (19)$$

$$i_{C1} = i_P - i_{DC}; \quad i_P = (S_P + S_{CP})i_F \quad (20)$$

$$i_{C2} = -i_N - i_{DC}; \quad i_N = (S_N + S_{CN})i_F, \quad (21)$$

where all four possible switching states are handled together, as suggested for the general case in (10)–(12). Furthermore, by virtue of (20), (21) and (17), it is found that

$$i_G = i_{C1} - i_{C2} = (S_P + S_N + S_{CP} + S_{CN})i_F = i_F. \quad (22)$$

As pointed out in Section 3.2, extending this analysis to a 3L FC converter of any number of legs, N_{legs} , is trivial. In this particular case, in which $N_{legs} = 4$ —legs R, S, T and U —, the (18)–(22) set turns, equation by equation, into the (23)–(27) set given next:

$$U_{Fj} = (S_{jCN} - S_{jCP})U_{Cj} + (S_{jP} + S_{jCP})U_{C1} - (S_{jN} + S_{jCN})U_{C2}; \quad j = R, S, T, U \quad (23)$$

$$i_{Cj} = (S_{jCN} - S_{jCP})i_{Fj}; \quad j = R, S, T, U \quad (24)$$

$$i_{C1} = i_P - i_{DC}; \quad i_P = \sum_{j=R,S,T,U} (S_{jP} + S_{jCP})i_{Fj} \quad (25)$$

$$i_{C2} = -i_N - i_{DC}; \quad i_N = \sum_{j=R,S,T,U} (S_{jN} + S_{jCN})i_{Fj} \quad (26)$$

$$i_G = \sum_{j=R,S,T,U} i_{Fj}. \quad (27)$$

Even though expressions (23)–(27) fully describe the 4L-3L FC operation, they must be associated to the dynamic models of both the AC filter and the accumulative components to define a state-space representation of the whole system displayed in Fig. 2. Specifically, the equations linking the AC grid voltage and current to the output of the LCL filter in Fig. 2 turn out to be

$$V_{Gj} = U_{CFj} + R_{Gj}i_{Gj} + L_{Gj} \frac{di_{Gj}}{dt}; \quad j = R, S, T, U \quad (28)$$

$$U_{Fj} = U_{CFj} - R_{Fj}i_{Fj} - L_{Fj} \frac{di_{Fj}}{dt}; \quad j = R, S, T, U \quad (29)$$

$$C_{Fj} \frac{dU_{CFj}}{dt} = i_{Gj} - i_{Fj}; \quad j = R, S, T, U. \quad (30)$$

As far as the capacitors of the converter and the DC-link are concerned, their corresponding dynamics are modeled as

$$C_j \frac{dU_{Cj}}{dt} = i_{Cj}; \quad j = R, S, T, U \quad (31)$$

$$C_1 \frac{dU_{c1}}{dt} = i_{c1} \quad (32)$$

$$C_2 \frac{dU_{c2}}{dt} = i_{c2}. \quad (33)$$

Solving for di_{Gj}/dt in (28) gives rise to the following first set of four state equations:

$$\frac{di_{Gj}}{dt} = -\frac{R_{Gj}}{L_{Gj}} i_{Gj} - \frac{1}{L_{Gj}} U_{CFj} + \frac{1}{L_{Gj}} V_{Gj}; \quad j = R, S, T, U. \quad (34)$$

Moreover, equating (23) to (29), and subsequently solving for di_{Fj}/dt , produces

$$\begin{aligned} \frac{di_{Fj}}{dt} = & -\frac{R_{Fj}}{L_{Fj}} i_{Fj} + \frac{1}{L_{Fj}} U_{CFj} - \frac{1}{L_{Fj}} (S_{CNj} - S_{CPj}) U_{Cj} - \frac{1}{L_{Fj}} (S_{Pj} + S_{CPj}) U_{C1} \\ & + \frac{1}{L_{Fj}} (S_{Nj} + S_{CNj}) U_{C2}; \quad j = R, S, T, U \end{aligned} \quad (35)$$

The last set of four state equations arising from the LCL filter is derived from (30) as follows:

$$\frac{dU_{CFj}}{dt} = \frac{1}{C_{Fj}} i_{Gj} - \frac{1}{C_{Fj}} i_{Fj}; \quad j = R, S, T, U. \quad (36)$$

On the other hand, replacing (24) into (31) leads to

$$\frac{dU_{Cj}}{dt} = \frac{1}{C_j} (S_{jCN} - S_{jCP}) i_{Fj}; \quad j = R, S, T, U. \quad (37)$$

Finally, the last two state equations provided next are derived by substituting (25) and (26) into, respectively, (32) and (33):

$$\frac{dU_{c1}}{dt} = \frac{1}{C_1} \sum_{j=R,S,T,U} (S_{jP} + S_{jCP}) i_{Fj} - \frac{1}{C_1} i_{DC} \quad (38)$$

$$\frac{dU_{c2}}{dt} = -\frac{1}{C_2} \sum_{j=R,S,T,U} (S_{jN} + S_{jCN}) i_{Fj} - \frac{1}{C_2} i_{DC}. \quad (39)$$

It should be noticed that (27) is merely informative and does not contribute to any additional state equation. In any case, if required, it might be incorporated to the state-space model as an output equation.

Aiming at rearranging the (34)–(39) state equation set according to the matrix form in (13), the \mathbf{d}_A and \mathbf{d}_B disturbance subvectors defined in (6) are found to be

$$\mathbf{d}_A = [V_{GR} \ V_{GS} \ V_{GT} \ V_{GU}]^T; \quad \mathbf{d}_B = [i_{DC}], \quad (40)$$

while the \mathbf{x}_A , \mathbf{x}_{con} and \mathbf{x}_B state subvectors are as follows:

$$\mathbf{x}_A = [i_{GR} \ i_{GS} \ i_{GT} \ i_{GU} \ i_{FR} \ i_{FS} \ i_{FT} \ i_{FU} \ U_{CFR} \ U_{CFS} \ U_{CFT} \ U_{CFU}]^T \quad (41)$$

$$\mathbf{x}_{con} = [U_{CR} \ U_{CS} \ U_{CT} \ U_{CU}]^T; \quad \mathbf{x}_B = [U_{C1} \ U_{C2}]^T. \quad (42)$$

Considering the disturbance and state vectors arising, respectively, from (40) and (41)–(42), both the $\mathbf{A}(\mathbf{u})$ and \mathbf{E} matrices in (13) can be straightforwardly derived from (34)–(39). For that purpose, let us define

$$\left. \begin{array}{l} \tau_{Gj} = \frac{R_{Gj}}{L_{Gj}} \\ \tau_{Fj} = \frac{R_{Fj}}{L_{Fj}} \\ \Delta_j(\mathbf{u}) = S_{jCN} - S_{jCP} \\ \Sigma_j(\mathbf{u}) = S_{jP} + S_{jCP} \\ \Gamma_j(\mathbf{u}) = S_{jN} + S_{jCN} \end{array} \right\}; \quad j = R, S, T, U. \quad (43)$$

Furthermore, for any phase-repeated parameter or variable, $\lambda_j; j = R, S, T, U$, let us also define

$$\boldsymbol{\lambda} = \begin{bmatrix} \lambda_R \\ \lambda_S \\ \lambda_T \\ \lambda_U \end{bmatrix}; \quad \text{diag}(\boldsymbol{\lambda}) = \begin{bmatrix} \lambda_R & 0 & 0 & 0 \\ 0 & \lambda_S & 0 & 0 \\ 0 & 0 & \lambda_T & 0 \\ 0 & 0 & 0 & \lambda_U \end{bmatrix}. \quad (44)$$

Then, considering (43) and (44), the nine submatrices in which $\mathbf{A}(\mathbf{u})$ is divided in (7) turn out to be

$$\mathbf{A}_{AA} = \begin{bmatrix} \text{diag}(-\boldsymbol{\tau}_G) & \mathbb{O}_{4 \times 4} & \text{diag}\left(-\frac{1}{L_G}\right) \\ \mathbb{O}_{4 \times 4} & \text{diag}(-\boldsymbol{\tau}_F) & \text{diag}\left(\frac{1}{L_F}\right) \\ \text{diag}\left(\frac{1}{C_F}\right) & \text{diag}\left(-\frac{1}{C_F}\right) & \mathbb{O}_{4 \times 4} \end{bmatrix} \quad (45)$$

$$\mathbf{A}_{concon} = \mathbb{O}_{4 \times 4}; \quad \mathbf{A}_{BB} = \mathbb{O}_{2 \times 2} \quad (46)$$

$$\mathbf{A}_{Acon}(\mathbf{u}) = \begin{bmatrix} \mathbb{O}_{4 \times 4} \\ \text{diag}\left(-\frac{\boldsymbol{\Delta}(\mathbf{u})}{L_F}\right) \\ \mathbb{O}_{4 \times 4} \end{bmatrix}; \quad \mathbf{A}_{conA}(\mathbf{u}) = \begin{bmatrix} \mathbb{O}_{4 \times 4} \\ \text{diag}\left(\frac{\boldsymbol{\Delta}(\mathbf{u})}{C}\right) \\ \mathbb{O}_{4 \times 4} \end{bmatrix}^T \quad (47)$$

$$\mathbf{A}_{AB}(\mathbf{u}) = \begin{bmatrix} \mathbb{O}_{4 \times 1} & \mathbb{O}_{4 \times 1} \\ -\frac{\boldsymbol{\Sigma}(\mathbf{u})}{L_F} & \frac{\boldsymbol{\Gamma}(\mathbf{u})}{L_F} \\ \mathbb{O}_{4 \times 1} & \mathbb{O}_{4 \times 1} \end{bmatrix}; \quad \mathbf{A}_{BA}(\mathbf{u}) = \begin{bmatrix} \mathbb{O}_{4 \times 1} & \mathbb{O}_{4 \times 1} \\ \frac{1}{C_1} \boldsymbol{\Sigma}(\mathbf{u}) & -\frac{1}{C_2} \boldsymbol{\Gamma}(\mathbf{u}) \\ \mathbb{O}_{4 \times 1} & \mathbb{O}_{4 \times 1} \end{bmatrix}^T \quad (48)$$

$$\mathbf{A}_{conB} = \mathbb{O}_{4 \times 2}; \quad \mathbf{A}_{Bcon} = \mathbb{O}_{2 \times 4}. \quad (49)$$

Likewise, the \mathbf{E} matrix given next is derived:

$$\mathbf{E} = \begin{bmatrix} \text{diag}\left(\frac{1}{L_G}\right) & \mathbb{O}_{4 \times 1} \\ \mathbb{O}_{12 \times 4} & \mathbb{O}_{12 \times 1} \\ \mathbb{O}_{1 \times 4} & -\frac{1}{C_1} \\ \mathbb{O}_{1 \times 4} & -\frac{1}{C_2} \end{bmatrix}. \quad (50)$$

4.3. Simulation results

In order to validate the model presented above, it faces a Simscape Power System™ simulation model also reproducing the case study represented through Figs. 2 and 3, only with realistic power switches, modeled with a non null internal resistance and a non-infinite snubber capacitance, instead of the ideal ones considered when designing the SSSR. The AC grid considered is modeled by means of a balanced ideal star-connected three-phase generator plus neutral leg, whereas the DC link is portrayed as an infinite load fixing the current in its branch. The electrical parameters considered for the overall system, which have been adopted

from [19], are those displayed in Table II.

TABLE II
NUMERICAL VALUES OF THE PARAMETERS

Parameter	Value	Unit
R_{Fj}	10	Ω
R_{Gj}	10	Ω
L_{Fj}	30	mH
L_{Gj}	30	mH
C_{Fj}	1	mF
C_j	1	mF
C_1	3.3	mF
C_2	3.3	mF
V_{Gj}	230	V (rms)

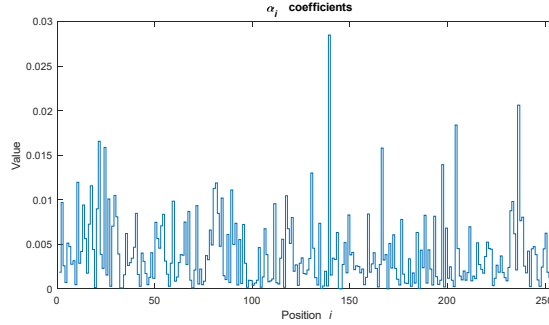


Fig. 4. One combination of coefficients leading to a stable equivalent system

i_{DC}	10	A
T	100	μs

As suggested in Section 2.2, each of the $N = N_{poss}^{N_{legs}} = 4^4 = 256$ possible switching states of the 4L-3L FC converter leads to a different subsystem, characterized by its corresponding constant A_i matrix, where $i = 1, 2, 3 \dots 256$. In this context, bearing in mind the parameter values provided in Table II, analysis of the eigenvalues for each of those 256 A_i matrices reveals that 4 of them correspond to asymptotically stable subsystems, while 66 represent unstable subsystems. The remaining 186 yield potentially unstable subsystems, strictly in the limit between stability and instability.

In spite of this, the existence of a commutation sequence stabilizing the system has been confirmed through completion of the condition provided in Section 2.2. In fact, several weight vectors generated to satisfy (4) and leading to stable equivalent systems in the sense of (5)

have been found. For example, selecting the weight vector whose α_i elements are those described in Fig. 4, the equivalent system computed as specified in (5), turns out to be stable,

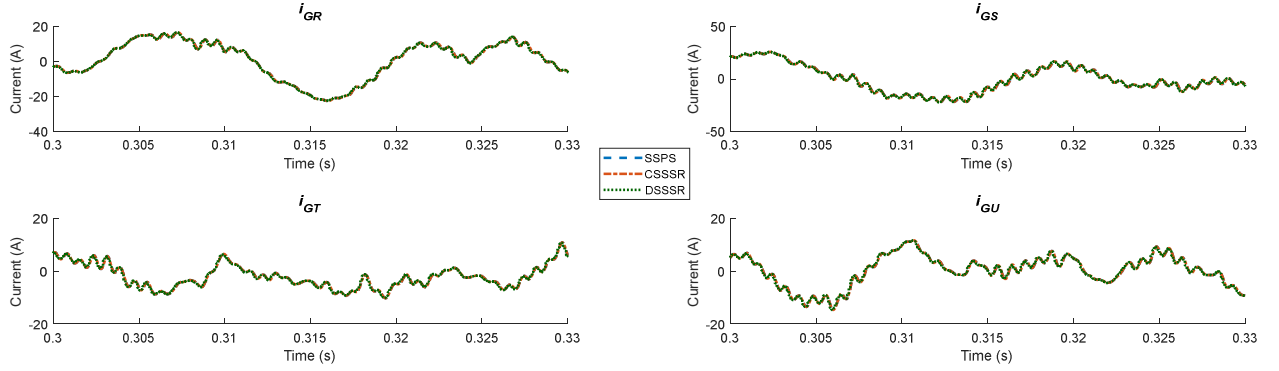


Fig. 5. Currents flowing through the L_{Gj} inductances of the grid filter

as demanded by Lyapunov's theorem.

On the other hand, application of the ZOH discretization method described in Section 3.3 leads to the discrete-time equivalent model of the continuous SSSR given by (45)–(50). An eventual MPC algorithm should rest on the discrete-time SSSR, which is also made of 256 subsystems. When adopting the 100- μ s sample time reflected in Table II, 5 of those subsystems are asymptotically stable, while 42 of them are unstable and the remaining 209 happen to be in the limit between stability and instability.

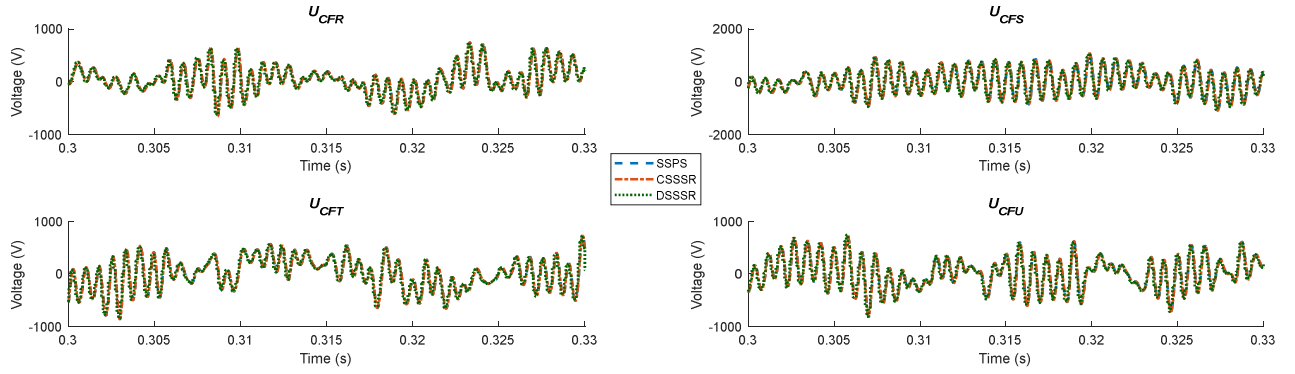


Fig. 7. Voltages across the terminal of the grid filter capacitors

Aiming at assessing the accuracy of the SSSR, its continuous and discrete-time versions are compared with each other as well as with the aforementioned SPSM. All three models — SPSM, CSSSR and DSSSR—undergo identical disturbance inputs and are driven by the same control sequence, generated by a MPC controller.

Figures 5 to 9 present the dynamic responses of the eighteen state variables of the system under study when excited by the uncontrolled $V_{Gj}; j = R, S, T, U$, and i_{DC} inputs presented in Table II and the control input depicted in Fig. 10. Incidentally, the cost function of the MPC controller generating the control sequence has been chosen to cover a large spectrum of possible switching positions, and is not relevant in terms of control.

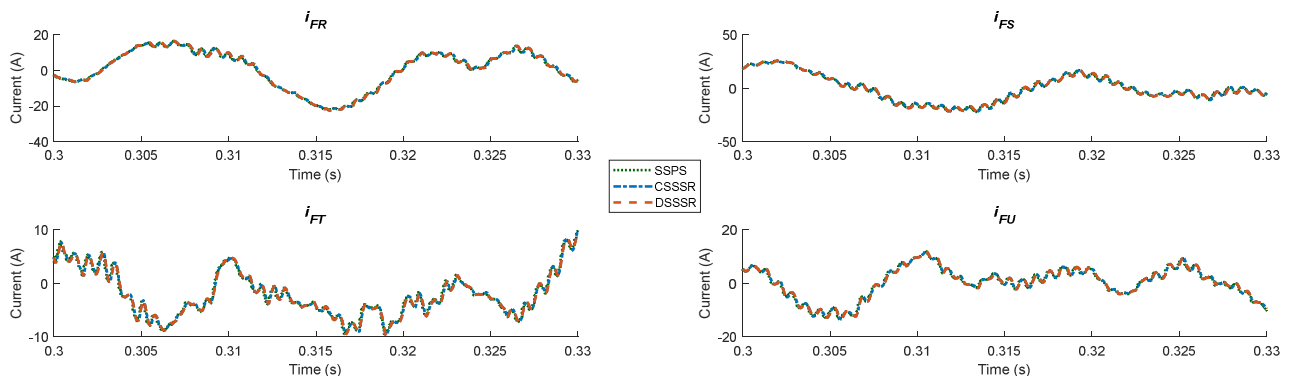


Fig. 6. Currents flowing through the L_{Fj} inductances of the grid filter

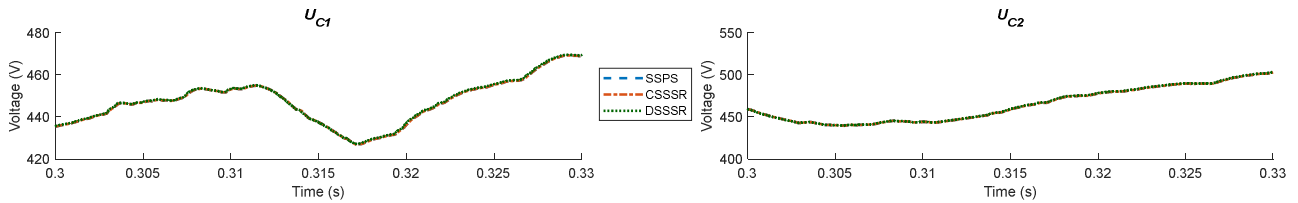


Fig. 9. Voltages across the terminals of the DC-link capacitors

Specifically, only a 30-millisecond window of the 4-second test performed is displayed, during which a particularly high number of the 256 possible switching states takes place spontaneously. The scale chosen is also coherent with the problem of error propagation mentioned in section 2.3, as it is still close enough to the initial time not to have noticeable errors. For each state variable, the proximity between the performances of the three models is put in evidence. Juxtaposition, in each subfigure, of the signals coming from all three simulation models allows validating the modeling technique proposed in this paper. It also corroborates the suitability of the discretization method selected, as the discrete and continuous systems are coherently obeying the same dynamics.

However, certain discrepancies also appear. Though minor, they are due to several reasons. First of all, the complexity of SPSM model is different, as it considers phenomena not dealt

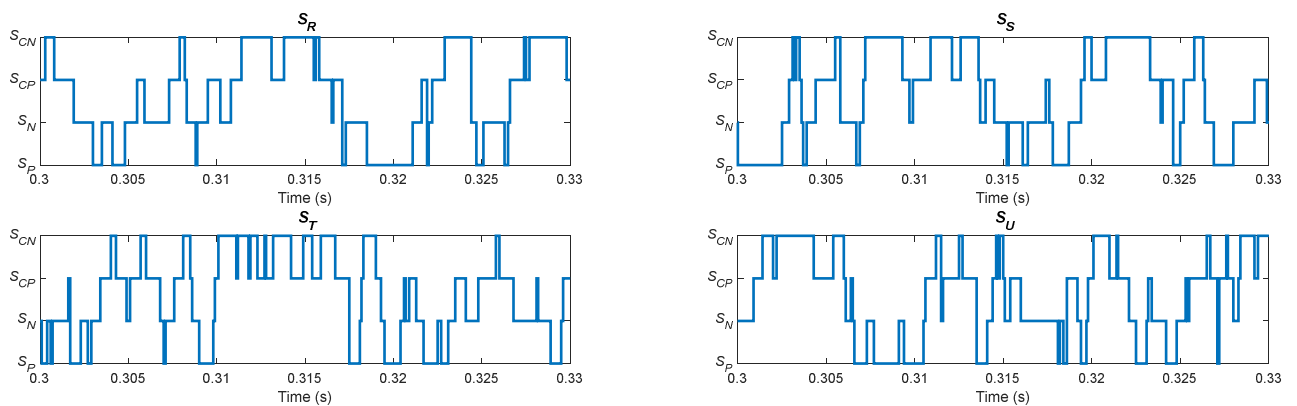


Fig. 10. Switching states for each commutation cell



Fig. 8. Voltages across the terminals of the four inner capacitors

with in the other two models. In this respect, it is worth noting that, as far as the CSSSR is concerned, its switching electronic devices have been deliberately modeled as ideal switches. Such an approximation allows keeping the required balance between accurateness and computational feasibility of the DSSSR, given that the discrete model has been expressly conceived to efficiently drive the prediction stage of a MPC algorithm. It is also interesting to note that the commutation frequency is rather high, up to 10 kHz, and that it may exacerbate the differences between models, as the imposed dynamics are particularly fast. Finally, it must be considered that all definitions of subsystems lead theoretically to possible errors when spanning from one given subsystem to another. Considering all these factors, the results are overall fitting for a control model.

5. Conclusion

This paper focuses on a universal method to generate accurate state-space models, adapted from switched state-space representation, allowing modeling of all power converters and their applications. Coupled with a methodical model predictive control algorithm based on graph theory, this methodology can be adopted to control power converters down to their power switches, enabling a deeper mastery of the system.

Additionally, the resulting control structure intrinsically adapts to virtually any context, topology or requirement, unlocking a great variety of applications, which fits perfectly the domain of power conversion. Nevertheless, the model described is an unusual variation on state-space representation, leading to new definition and study difficulties. This modeling approach is an important piece of the path to more efficient, more reliable and more intelligent power converters.

The effectiveness of the proposed modeling method has been validated through several simulations based on a 4L-3L FC topology, and a simple effective technique has been applied to investigate the stability of such a system. Because of the specificity of the proposed SSSR

for power converters, controllability and observability require additional studies and will be the subject of future investigations.

ACKNOWLEDGMENTS

The authors gratefully acknowledge the financial support of:

- Nouvelle Aquitaine Region and BPI France through the Insul'Grid project.
- The Spanish Ministry of Economy and Business (research project DPI2015-64985-R).
- The FEDER Funds, EU.
- The University of the Basque Country UPV/EHU (research grant GIU16/54).
- The Basque Government (research grant IT1256-19).

REFERENCES

- [1] K. Ma, *Power Electronics for the Next Generation Wind Turbine System*, London, UK: Springer, 2015.
- [2] F. Blaabjerg and K. Ma, "Future on power electronics for wind turbine systems," *IEEE J. Emerging Sel. Topics Power Electron.*, vol. 1, no. 3, pp. 139–152, Sep. 2013.
- [3] S. Ceballos, J. Pou, J. Zaragoza, J. L. Martín, E. Robles, I. Gabiola, and P. Ibáñez, "Efficient modulation technique for a four-leg fault-tolerant neutral-point-clamped inverter," *IEEE Trans. Ind. Electron.*, vol. 55, no. 3, pp. 1067–1074, Mar. 2008.
- [4] H. Wang, M. Liserre, and F. Blaabjerg, "Toward reliable power electronics: Challenges, design tools, and opportunities," *IEEE Ind. Electron. Mag.*, vol. 7, no. 2, pp. 17–26, Jun. 2013.
- [5] M. Tsili and S. Papathanassiou, "A review of grid code technical requirements for wind farms," *IET Renew. Power Gener.*, vol. 3, no. 3, pp. 308–332, Sep. 2009.
- [6] K. Katsavounis, P. Hou, W. Hu, and Z. Chen, "Optimal energy flow in islanded integrated energy systems," in *Proc. IECON 2017 - 43rd Annual Conference of the IEEE Industrial Electronics Society*, Beijing, 2017, pp. 369–374.
- [7] R. Teodorescu, M. Liserre, and P. Rodríguez, *Grid Converters for Photovoltaic and Wind Power Systems*, New York, USA: Wiley-IEEE Press, 2011.
- [8] D. G. Holmes and T. A. Lipo, *Pulse Width Modulation for Power Converters: Principles and Practice*, New York, USA: Wiley-IEEE Press, 2003.
- [9] J. Zaragoza, J. Pou, S. Ceballos, E. Robles, P. Ibáñez, and J. L. Villate, "A comprehensive study of a hybrid modulation technique for the neutral-point-clamped converter," *IEEE Trans. Ind. Electron.*, vol. 56, no. 2, pp. 294–304, Feb. 2009.
- [10] A. Susperregui, M. I. Martínez, G. Tapia, and I. Vechiu, "Second-order sliding-mode controller design and tuning for grid synchronisation and power control of a wind turbine-driven doubly fed induction generator," *IET Renew. Power Gener.*, vol. 7, no. 5, pp. 540–551, Sep. 2013.
- [11] A. Susperregui, J. Jugo, I. Lizarraga, and G. Tapia, "Automated control of doubly fed induction generator integrating sensorless parameter estimation and grid synchronisation," *IET Renew. Power Gener.*, vol. 8, no. 1, pp. 76–89, Jan. 2014.
- [12] M. I. Martínez, A. Susperregui, and G. Tapia, "Second-order sliding-mode-based global control scheme for wind turbine-driven DFIGs subject to unbalanced and distorted grid voltage," *IET Electr. Power Appl.*, vol. 11, no. 6, pp. 1013–1022, Jul. 2017.
- [13] S.-C. Tan, Y. M. Lai, and C. K. Tse, "Indirect sliding mode control of power converters via double integral sliding surface," *IEEE Trans. Power Electron.*, vol. 23, no. 2, pp. 600–611, Mar. 2008.
- [14] S. Jupin, I. Vechiu, and G. Tapia, "Direct state-space model for model predictive control of multi-level power converters," in *Proc. IECON 2017 - 43rd Annual Conference of the IEEE Industrial Electronics Society*, Beijing, 2017, pp. 7759–7764.
- [15] P. Cortés, J. Rodríguez, D. Quevedo, and C. Silva, "Predictive current control strategy with imposed load current spectrum," in *Proc. 2006 12th International Power Electronics and Motion Control Conference*, Portorož, 2006, pp. 252–257.
- [16] S. Kouro, P. Cortés, R. Vargas, U. Ammann, and J. Rodríguez, "Model predictive control – a simple and powerful method to control power converters," *IEEE Trans. Ind. Electron.*, vol. 56, no. 6, pp. 1826–1838, Jun. 2009.
- [17] M. Pereira, D. Limon, T. Alamo, and L. Valverde, "Application of periodic economic MPC to a grid-connected micro-grid," in *Proc. 5th IFAC Conference on Nonlinear Model Predictive Control*, Seville, 2015, pp. 514–519.
- [18] K. Antoniewicz, M. Jasinski, M. P. Kazmierkowski, and M. Malinowski, "Model predictive control for three-level four-leg flying capacitor converter operating as shunt active power filter," *IEEE Trans. Ind. Electron.*, vol. 63, no. 8, pp. 5255–5262, Aug. 2016.
- [19] R. Vargas, P. Cortés, U. Ammann, J. Rodríguez, and J. Pontt, "Predictive control of a three phase neutral-point-clamped inverter," *IEEE Trans. Ind. Electron.*, vol. 54, no. 5, pp. 2697–2705, Oct. 2007.
- [20] R. Zaimeddine and T. Undeland, "Direct power control strategies of a grid-connected three-level voltage source converter VSI-NPC," in *Proc. 2011 14th European Conference on Power Electronics and Applications*, Birmingham, 2011, pp. 1–7.
- [21] C. Valentin, M. Magos, and B. Maschke, "A port-Hamiltonian formulation of physical switching systems with varying constraints," *Automatica*, vol. 43, no. 7, pp. 1125–1133, Jul. 2007.
- [22] F. El Hachemi, M. Sigalotti, and J. Daafouz, "Stability analysis of singularly perturbed switched linear systems," *IEEE Trans. Automat. Contr.*, vol. 57, no. 8, pp. 2116–2121, Aug. 2012.

Corresponding author: Samuel Jupin, Univ. Bordeaux, ESTIA Institute of technology, University of the Basque Country UPV/EHU, s.jupin@estia.fr

- [23] R. A. DeCarlo, M. S. Branicky, S. Pettersson, and B. Lennartson, "Perspectives and results on the stability and stabilizability of hybrid systems," *Proc. IEEE*, vol. 88, no. 7, pp. 1069–1082, Jul. 2000.
- [24] D. Liberzon, *Switching in Systems and Control*, Boston, USA: Birkhäuser Boston Inc., 2003.
- [25] M. Wicks, P. Peleties, and R. DeCarlo, "Construction of piece-wise Lyapunov functions for stabilizing switched systems," in *Proc. 33rd IEEE Conference on Decision and Control*, Orlando, 1994, pp. 3492–3497.
- [26] M. Wicks, P. Peleties, and R. DeCarlo, "Switched controller synthesis for the quadratic stabilization of a pair of unstable linear systems," *Eur. J. Contr.*, vol. 4, no. 2, pp. 140–147, Feb. 1998.
- [27] A. Bemporad and M. Morari, "Robust model predictive control: A survey," in *Robustness in identification and control*, A. Garulli and A. Tesi, Eds. London: Springer London, 1999, pp. 207–226.

TABLES AND FIGURES

TABLE I
RELATION BETWEEN THE IGBTs' STATE AND THE CONNECTION VARIABLE

S_j	S_1	S_2	S_3	S_4	Connection
S_P	1	1	0	0	P
S_N	0	0	1	1	N
S_{CP}	1	0	1	0	P, via C
S_{CN}	0	1	0	1	N, via C

TABLE II
NUMERICAL VALUES OF THE PARAMETERS

Parameter	Value	Unit
R_{Fj}	10	Ω
R_{Gj}	10	Ω
L_{Fj}	30	mH
L_{Gj}	30	mH
C_{Fj}	1	mF
C_j	1	mF
C_1	3.3	mF
C_2	3.3	mF
V_{Gj}	230	V (rms)
i_{DC}	10	A
T	100	μs

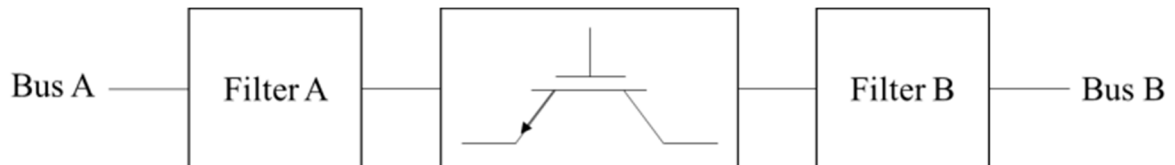


Fig. 1. General context of power conversion. Two buses, A and B, are connected through a filter + commutation cell system.

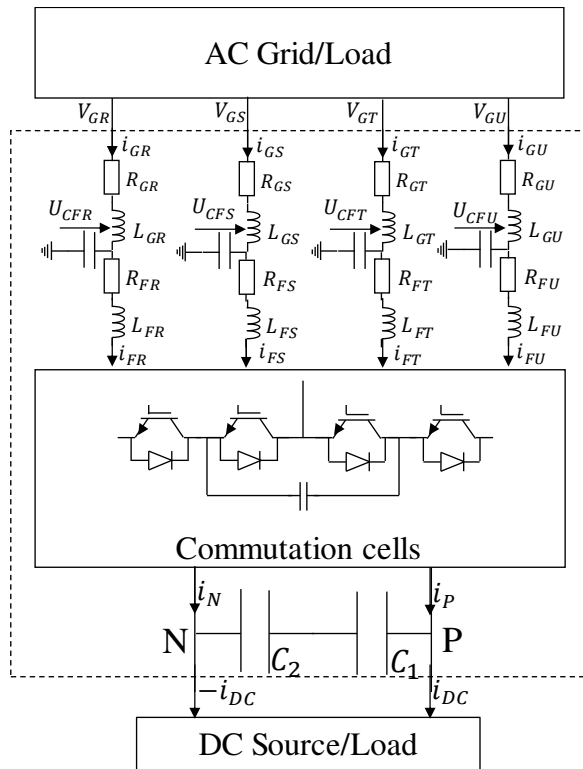


Fig. 2. Overview of the context of the study in which the modeled system is framed.

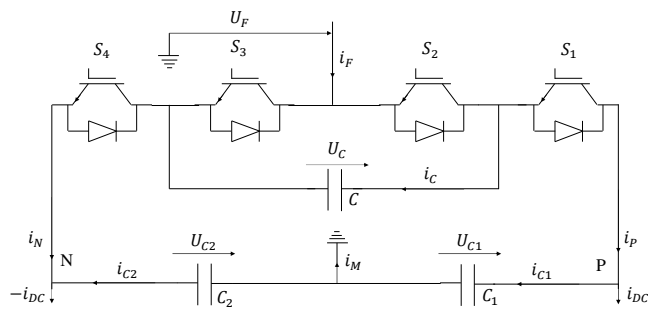


Fig. 3. Commutation cell and DC-link of the Flying Capacitor with i_F and U_F , respectively, the output current and voltage of the AC filter.

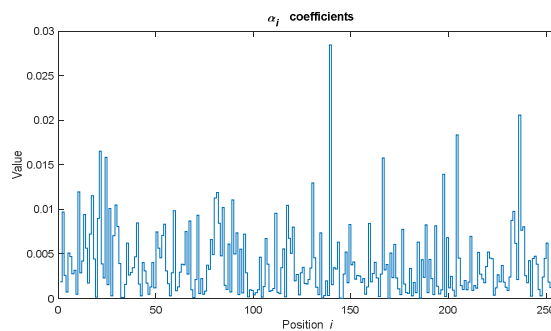


Fig. 4. One combination of coefficients leading to a stable equivalent system

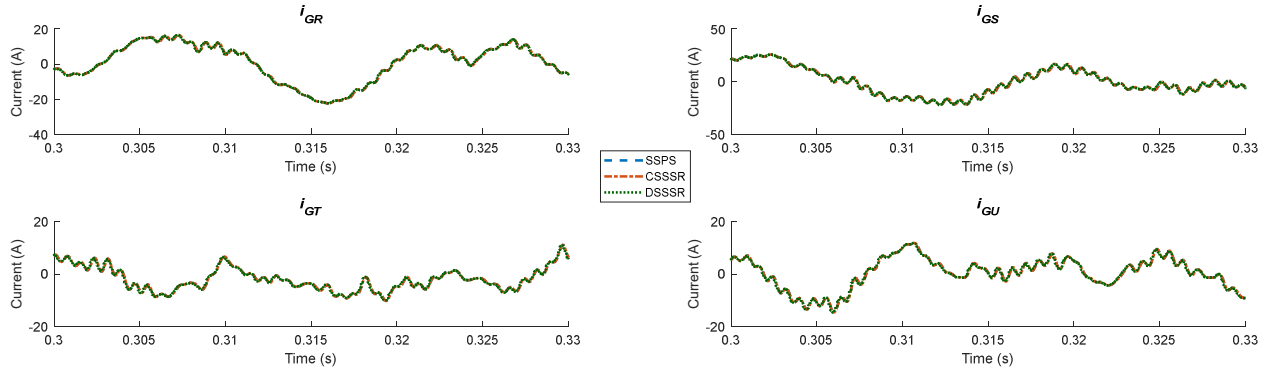


Fig. 5. Currents flowing through the L_{Gj} inductances of the grid filter

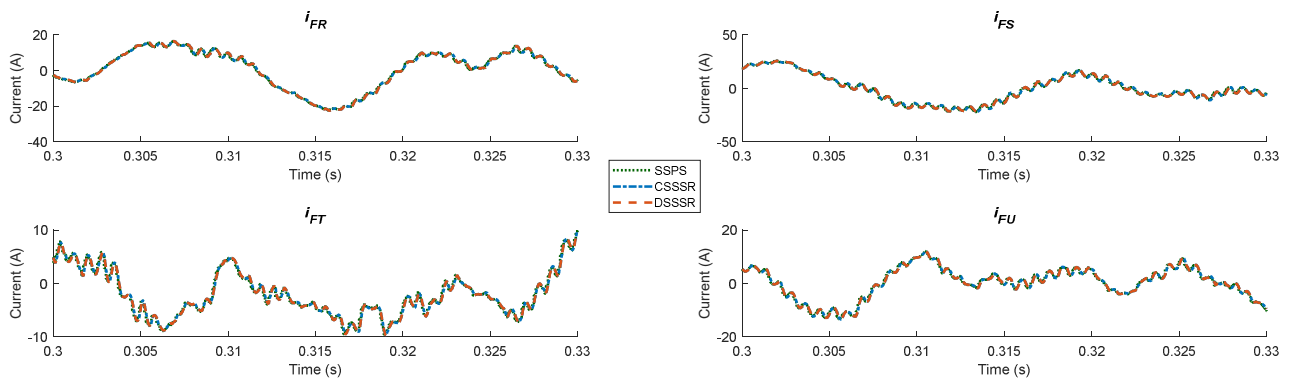


Fig. 6. Currents flowing through the L_{Fj} inductances of the grid filter

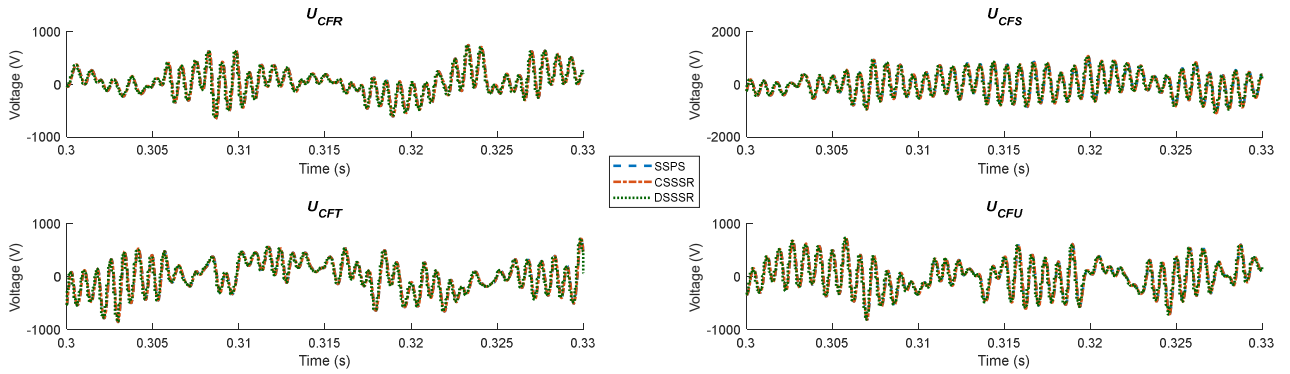


Fig. 7. Voltages across the terminal of the grid filter capacitors

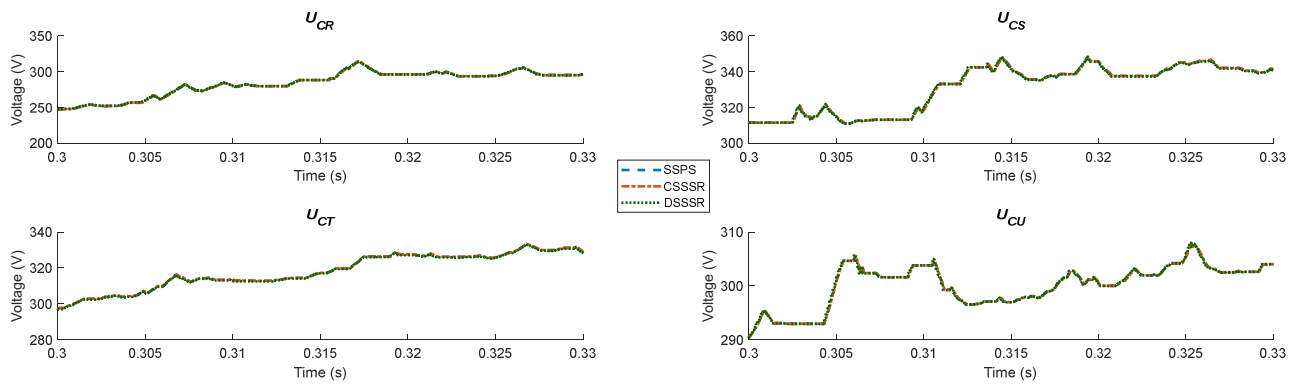


Fig. 8. Voltages across the terminals of the four inner capacitors

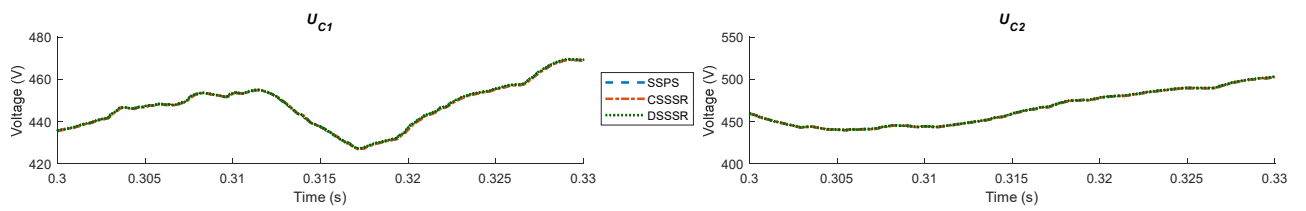


Fig. 9. Voltages across the terminals of the DC-link capacitors

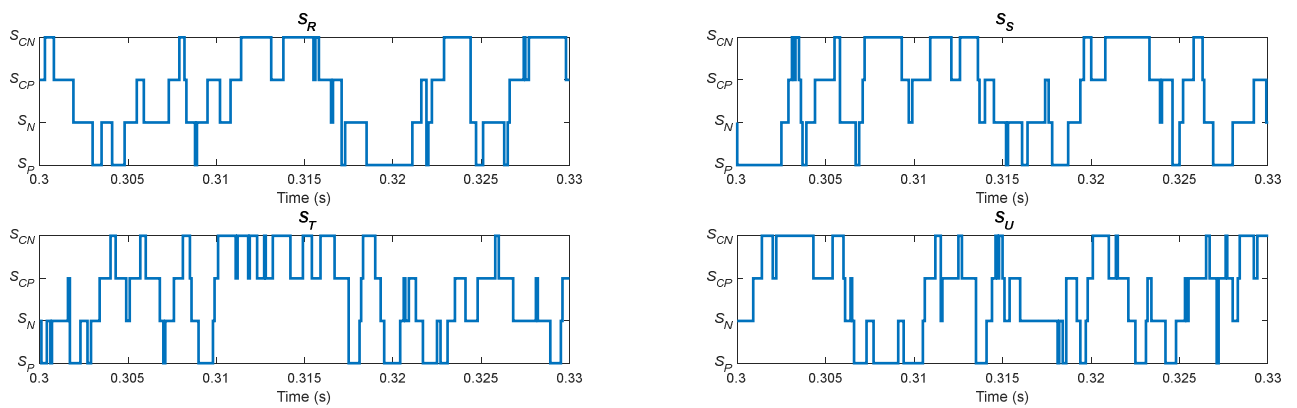


Fig. 10. Switching states for each commutation cell